Chemical Science

ROYAL SOCIETY OF CHEMISTRY

EDGE ARTICLE

View Article Online
View Journal | View Issue

Cite this: *Chem. Sci.*, 2022, **13**, 5597

All publication charges for this article have been paid for by the Royal Society of Chemistry

Access to tetracoordinate boron-doped polycyclic aromatic hydrocarbons with delayed fluorescence and aggregation-induced emission under mild conditions†

Long Jiang,[a] Yu Wang,[b] Dehui Tan,[a] Xiaobin Chen,[a] Tinghao Ma,[a] Baoliang Zhang *[a] and Deng-Tao Yang *[a]

Received 25th March 2022
Accepted 12th April 2022

DOI: 10.1039/d2sc01722a

rsc.li/chemical-science

Boron-doped polycyclic aromatic hydrocarbons (PAHs) have attracted ongoing attention in the field of optoelectronic materials due to their unique optical and redox properties. To investigate the effect of tetracoordinate boron in PAHs bearing N-heterocycles (indole and carbazole), a facile approach to four-coordinate boron-doped PAHs was developed, which does not require elevated temperature and pre-synthesized functionalized boron reactants. Five tetracoordinate boron-doped PAHs (**NBNN-1**–**NBNN-5**) were synthesized with different functional groups. Two of them (**NBNN-1** and **NBNN-2**) could further undergo oxidative coupling reactions to form fused off-plane tetracoordinate boron-doped PAHs **NBNN-1f** and **NBNN-2f**. The investigation of photophysical properties showed that the UV/vis absorption and fluorescence emission are significantly red-shifted compared to those of the three-coordinate boron-doped counterparts. In addition, the emission of **NBNN-1**–**NBNN-3** consisted of prompt fluorescence and delayed fluorescence. The compounds **NBNN-1f** and **NBNN-2f** showed aggregation-induced emission.

Introduction

Chemically doping heteroatoms into aromatic compounds has proven to be one of the most effective methods to tune their optoelectronic properties and intermolecular interactions.[1–12] Due to the isoelectronic relationship between boron and carbon cations and between the boron–nitrogen (BN) unit and two carbon atom (CC) motif, boron becomes an important element that can induce novel and complementary properties.[13–21] BN-doped aromatic compounds have a long history of evolution since the first example of BN-arene was reported by Alfred Stock in 1926.[22] Much the same to many other topics of chemistry, not much attention was paid until the new millennium. Nowadays, the synthesis of BN-doped arenes has become one of the most popular topics in organic chemistry and materials chemistry, and numerous new BN-doped aromatic compounds have been synthesized and demonstrated to have very distinct properties in optoelectronic materials.[23–27] Representative applications of B-doped polycyclic aromatic hydrocarbons (PAHs) have been demonstrated in organic field-effect transistors (OFETs)[21,28–30] and organic light emitting diodes (OLEDs).[21,29,31–37] Particularly, since PAHs decorated with *para*-positioned boron and nitrogen atoms have been reported to show thermally activated delayed fluorescence (TADF) with narrow full-width at half-maximum (FWHM) of emission based on efficient HOMO–LUMO separation by the multiple resonance effect in 2016,[31] BN-doped PAHs have been extensively studied for the next-generation OLEDs.

With the further development of BN-PAH chemistry by advances in the synthetic methodology and by the application potential of BN-doped π-conjugated systems, attention to the structure–property relationship has arisen.[38,39] The location of the BN unit was found to be important for the optoelectronic properties because whether the BN unit could fully conjugate with PAHs is highly dependent on its locations.[40–44] Although both the number of BN units[45–50] and different orientations of BN units[6,51–54] are believed to exhibit non-negligible impact on the optoelectronic properties and intermolecular interactions, only a few of examples have been documented due to the limited synthetic methodology.

In addition, the majority of previous attention has been paid to the tricoordinate boron units in PAHs,[55–60] tetracoordinate boron has been viewed more as a functional group instead of a dopant.[61–66] In fact, the coordination number of the boron atom shows noteworthy impact on the photophysical

[a]*School of Chemistry and Chemical Engineering, Northwestern Polytechnical University, Xi'an, Shanxi 710072, China. E-mail: blzhang@nwpu.edu.cn; dtyang@nwpu.edu.cn*

[b]*School of Chemistry and Chemical Engineering, Beijing Institute of Technology, Beijing, 100081, China*

† Electronic supplementary information (ESI) available. CCDC 2128933 (**NBNN-1**), 2128995 (**NBNN-1f**), 2129008 (**NBNN-3**). For ESI and crystallographic data in CIF or other electronic format see https://doi.org/10.1039/d2sc01722a

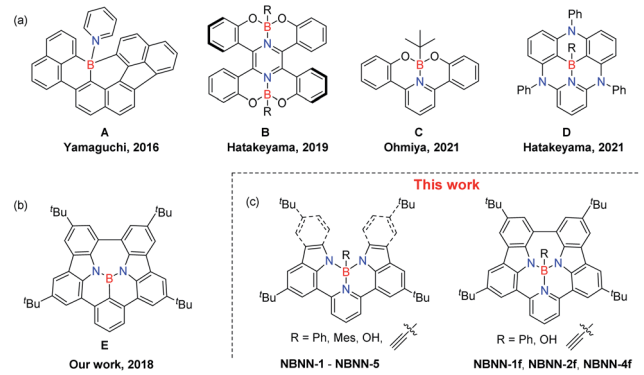

Scheme 1 Representative examples of tetracoordinate B-doped PAHs (a), our previous work (b) and chemical structures of this work (c).

properties. Recently, effort to replace the three-coordinate boron of the BN unit with four-coordinate boron has been made (Scheme 1a). The formation/dissociation of the four-coordinate boron unit through a dynamic B–N coordination bond in B-PAHs (**A**)[67–69] has been exploited for the solution-processed fabrication of semiconducting films of poorly soluble B-PAHs. Hatakeyama *et al.* reported tetracoordinate boron-fused helicenes (**B**)[70] as cathode active materials for lithium batteries. The photoexcitable borate (**C**),[71] which is structurally similar to **B**, can form an alkyl radical *via* single electron transfer. Very recently, Hatakeyama *et al.* replaced tri-coordinate boron by tetracoordinate boron to form compound **D**.[72]

With respect to the synthetic methodology of introducing boron atoms, electrophilic borylation as the symbolic reaction to synthesize borylated compounds has shown advantages in efficiency, scalability and avoidance of previous reagents. However, this type of electrophilic borylation requires high temperature with high boiling point solvents, which needs long reaction time and makes subsequent purification difficult.[18,73–76]

We have longstanding interest both in developing the synthetic methodology and applications of BN-doped PAHs.[77–80] We have developed photo-driven elimination reactions to generate BN-PAHs[77] and further expand this elimination using heat.[78] We also proposed a new strategy named exciton-driven elimination (EDE) to enable the *in situ* solid-state conversion of non-emissive tetracoordinate boron-substituted heterocycles to highly emissive BN-PAHs in OLEDs.[79] In addition, we recently demonstrated combination of electrophilic borylation and oxidative coupling to be a facile and viable approach to new NBN-doped molecular systems with tri-coordinate boron atoms (Scheme 1b).[80] In this work, we further disclose the strategy of combining electrophilic borylation and oxidative coupling for producing tetra-coordinate boron-doped PAHs. Unlike the typical electrophilic borylation driven by high temperature, our system can quickly undergo borylation at room temperature followed by addition of different nucleophilic reagents to build tetra-coordinate BN-PAHs bearing different functional groups on boron atoms (Scheme 1c).

Results and discussion

For the synthesis of tetracoordinate boron-doped PAHs **NBNN-1–NBNN-5**, we started from the commercially available 2,6-dibromopyridine, which could undergo the Suzuki coupling reaction with readily available 1-Bpin-carbazole and 7-Bpin-indole to produce the precursor compounds **1a** and **1b** in 90% and 46% yields, respectively (Scheme 2).

Our first attempt to introduce the boron atom using BBr_3 as the boron source with $^{i}Pr_2EtN$ in *o*-dichlorobenzene (*o*-DCB) at 180 °C was successful to produce phenyl group functionalized BN-PAH **NBNN-1** when phenylmagnesium bromide was used as the nucleophilic reagent. The existence of *o*-DCB makes the purification difficult. We tried to use several other solvents with lower boiling points at lower reaction temperatures, all of which generated the target compound **NBNN-1** with similar yields around 70%. Usually, the presence of the additive $^{i}Pr_2EtN$ is proven to be essential for the electrophilic borylation, but the absence of $^{i}Pr_2EtN$ did not show any influence on the borylation yield. To our delight, the reaction temperature was finally lowered down to room temperature without $^{i}Pr_2EtN$ in 78% yield (Scheme 2). In addition, the kind of nucleophile was also probed, and lithium reagents like phenyl lithium could produce compound **NBNN-1** in slightly lower yield. While we were preparing the manuscript, the synthesis of **NBNN-1** was reported at high temperature with $PhBCl_2$ and the additive $^{i}Pr_2EtN$.[81] Our mild conditions are probably ascribed to the existence the pyridyl group which could act as a directing group coordinating with BBr_3 and make the following borylation of N–H bonds less challenging. This process does not require to break the C–H bonds either. In addition, compared to the pre-functionalized boron reagents RBX_2 (X = Cl, Br), the commercially available BBr_3 has higher Lewis acidity and reactivity which also play a non-negligible role in the borylation reaction. The mild conditions without using high boiling point solvent make the purification of the product less disturbing. With the optimal conditions in hand, ethynylmagnesium bromide and mesitylmagnesium bromide were used as nucleophiles to generate compounds **NBNN-2** and **NBNN-3** in 58% and 69% yields, respectively. Compound **NBNN-4** was obtained when the reaction was quenched by water without adding any nucleophiles in single-figure yield, however, the yield of **NBNN-4** was significantly improved to 46% when $^{i}Pr_2EtN$ was used to quench

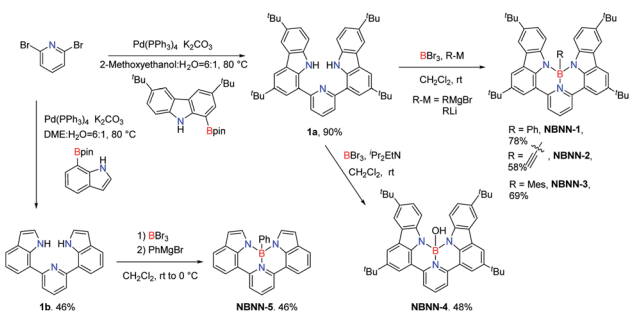

Scheme 2 Synthetic routes for NBNN-1 to NBNN-5.

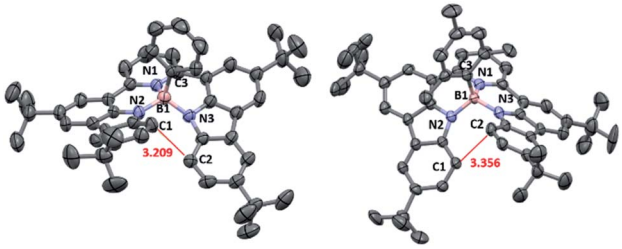

Fig. 1 Left: the crystal structure of **NBNN-1**. Important bond lengths (Å): C1–C2 3.209(5), B1–N1 1.653(4), B1–N2 1.508(5), B1–N3 1.541(5), and B1–C3 1.614(5). Right: the crystal structure of **NBNN-3**. Important bond lengths (Å): C1–C2 3.356(5), B1–N1 1.653(5), B1–N2 1.559(5), B1–N3 1.519(5), and B1–C3 1.634(6). Thermal ellipsoids are set at 50% probability. Hydrogen atoms are omitted for clarity.

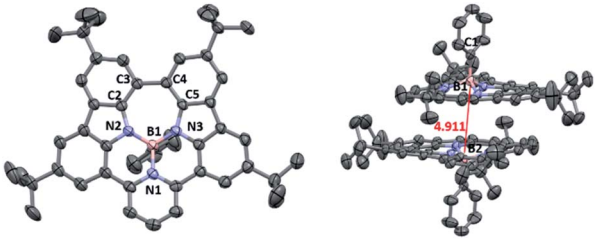

Fig. 2 Left: the crystal structure of **NBNN-1f** (50% thermal ellipsoids). Hydrogen atoms are omitted for clarity. Important bond lengths (Å): B1–B2: 4.911(4), B1–C1 1.613(4), B1–N1 1.640(4), B1–N2 1.523(4), B1–N3 1.502(3), N2–C2 1.397(4), C2–C3 1.404(4), C3–C4 1.510(4), C4–C5 1.409(5), and C5–N3 1.402(3).

the reaction. We also tried other hydroxy group containing reagents like phenol, which did not give the corresponding product at all. Compound **NBNN-5** based on two indole fragments was also synthesized under the optimal conditions. Other nucleophiles like isopropylmagnesium bromide, vinylmagnesium bromide, and methyl lithium could also yield the corresponding tetracoordinate boron-doped PAHs, however, these compounds were slowly decomposing on the silica gel or alumina. Bulky nucleophiles like ^{t}butylmagnesium bromide did not react, probably due to the steric hindrance. Compounds **NBNN-1** to **NBNN-5** were fully characterized by NMR and HRMS spectroscopy. The molecular structures of **NBNN-1** and **NBNN-3** were further determined by single-crystal X-ray diffraction analysis and are shown in Fig. 1.

Similar to our previous work on synthesized tricoordinate boron-doped PAHs,[80] the proximity and the steric repulsion between the hydrogen atoms of flanking units in **NBNN-1** to **NBNN-4** make them undergo the oxidative coupling reaction to form the fused forms. By combining 2,3-dichloro-5,6-dicyano-1,4-benzoquinone (DDQ) as the oxidant and TfOH as the acid, the fully fused compounds **NBNN-1f**, **NBNN-2f** and **NBNN-4f** were successfully observed. Compounds **NBNN-1f** and **NBNN-2f** were obtained in isolated yields of 78% and 58%, respectively (Scheme 3). Silica gel or alumina column chromatography was not compatible with **NBNN-4f**, which decomposed on the silica gel or alumina and was only confirmed by HRMS. **NBNN-3** did not undergo the oxidative coupling reaction probably due to the longer distance (3.356 Å, Fig. 1) between two carbon atoms on the carbazole segments. Unlike the tricoordinate boron-doped PAH analogue (**E** in Scheme 1),[80] the crystal structure of **NBNN-1f** showed that the four-coordinated boron atom adopts a tetrahedral geometry, which makes the molecular structure

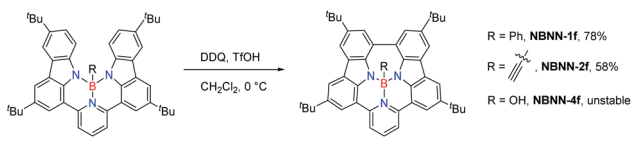

Scheme 3 Formation of fused tetracoordinate boron-doped PAHs *via* the oxidative coupling.

off-plane (Fig. 2). The B1–N1, B1–N2, and B1–N3 bond lengths are 1.640 Å, 1.523 Å, and 1.502 Å, respectively. Similar to tricoordinate boron-doped PAH **E**, the π-stacking interactions of **NBNN-1f** are limited to two neighbouring molecules with a longer separation distance than **E**.

The absorption, emission and electrochemical data of these seven tetracoordinate boron-doped PAHs are shown in Fig. 3 and Table 1. The absorption peaks are in agreement with the colors of their THF solutions (Fig. 3b). The general trend of the experimental absorption bands agrees with the time-dependent density functional theory (TD-DFT) calculations (Fig. 4, and see the ESI† for details). The broad absorption bands of **NBNN-1** to **NBNN-5** between 400 nm and 520 nm are ascribable to $S_0 \rightarrow S_1$ with transition configurations of HOMO → LUMO and $S_0 \rightarrow S_2$ with the major transition configuration of HOMO−1 → LUMO. Due to the closer energy gap between the HOMO and HOMO−1, **NBNN-1**, **NBNN-2** and **NBNN-5** only exhibited one peak at 469 nm, 465 nm and 446 nm, respectively. The smaller HOMO–LUMO gap results in red-shifted absorption peaks of **NBNN-3**, while the larger HOMO–LUMO gap brings about the blue-shifted absorption peaks of **NBNN-5**. The strong absorption peaks at 310 nm for **NBNN-1–NBNN-4** are likely attributed to the larger conjugation of the carbazole unit than the indole unit in **NBNN-5**. **NBNN-1f** and **NBNN-2f** showed five absorption bands with a maximum at $\lambda_{max} = 531$ nm and 528 nm which could be attributed to $S_0 \rightarrow S_1$ with the transition configuration of HOMO → LUMO, respectively. Different from **NBNN-1–NBNN-5**, the $S_0 \rightarrow S_2$ transitions of **NBNN-1f** at 457 nm and **NBNN-2f** at 439 nm consisted of HOMO → LUMO+1 with charge transfer character. Except **NBNN-5**, molecules **NBNN-1** to **NBNN-4** showed near-identical fluorescence spectra with emission peaks between 551 nm and 564 nm, which suggests that the substituents on the boron atom of tetracoordinate boron-doped PAHs have a negligible contribution to fluorescence. The fluorescent peaks in the poly(methyl methacrylate) (PMMA) film of **NBNN-1** to **NBNN-4** are very similar to those in THF solution, while the λ_{em} of **NBNN-5** in solid was red-shifted to 540 nm from bright green color to greenish yellow color as shown in Fig. 3b, which is probably because the less crowded structure of **NBNN-5** results in the π–π packing in the solid. The quantum yields both in solution and in the PMMA film of the open form of compounds bearing carbazole units are ~25%, except **NBNN-1**,

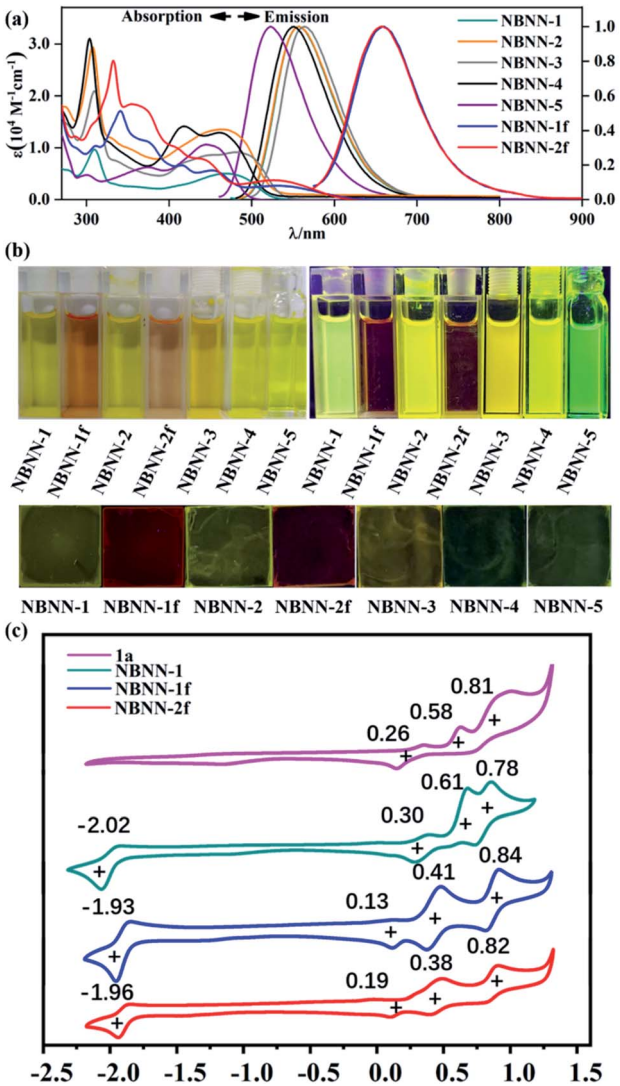

Fig. 3 (a) UV/vis and emission spectra of **NBNN-1** to **NBNN-5**, **NBNN-1f** and **NBNN-2f** in THF (10^{-5} M). (b) Photographs showing the colors (top left), fluorescent colors (top right) and PMMA films (bottom) of **NBNN-1** to **NBNN-5**, **NBNN-1f** and **NBNN-2f**. (c) Cyclic voltammograms of **1a**, **NBNN-1**, **NBNN-1f** and **NBNN-2f**: glassy carbon as the working electrode, and a Pt wire as reference and counter electrodes. Fc/Fc^+ = ferrocene/ferrocenium, ferrocene was added to the solution as the internal reference, scan rate = 100 mV s^{-1}.

which has much higher quantum yields in solution (Φ_{pl} = 62.3%) and PMMA film (Φ_{pl} = 55.7%) (Table 1). Compound **NBNN-5** bearing indole units only has less than 10% quantum yield both in solution and in solid probably due to vibrational relaxation caused by the less crowded structure. Compared to **NBNN-1** and **NBNN-2**, the emission peaks of the fused molecules **NBNN-1f** and **NBNN-2f** show remarkable red-shift up to 100 nm and exhibit indistinguishable fluorescent spectra (λ_{em} = 660 nm, Φ < 1%), while their absorption spectra are also similar with different absorption extinction coefficients. The fluorescence peak of **NBNN-1f** in the PMMA film was blue-shifted up to 39 nm compared to that in solution (see the ESI† for details), while **NBNN-2f** in the PMMA film exhibited two emission peaks at 624 nm and 659 nm. The blue-shifted emission peaks of **NBNN-1f** and **NBNN-2f** are probably ascribed to the structure constraint, which could also result in aggregation-induced emission (AIE). Both **NBNN-1f** and **NBNN-2f** showed a significant increase in quantum yields in solid up to 4%. The low quantum yields of **NBNN-1f** and **NBNN-2f** are likely due to the internal conversion between small S_0–S_1 gaps. The fluorescence peaks in solution and solid are consistent with the emission colors of their THF solutions and PMMA films (Fig. 3b). Ligand **1a** has two absorption bands at 294 nm and 364 nm, while Ligand **1b** has a broad band at 330 nm and a less intensive band at 364 nm (Fig. S5.16†). These two molecules **1a** and **1b** showed weak fluorescence with emission maxima at 636 nm and 656 nm, respectively. The quantum yields both in solution and in the PMMA film of the two molecules were less than 0.1%. Compared to the ligands, the boron-doped PAHs exhibited substantially red-shifted absorption spectra with enhanced emission quantum yields. As shown in Table 1 and Fig. S5.5–S5.11,† the phosphorescence decays at 77 K were recorded in the range of 200–400 ms for **NBNN-1**–**NBNN-5**, while the fused compounds **NBNN-1f** and **NBNN-2f** showed much shorter phosphorescence decays (0.012 ms and 5.62 ms, respectively).

The time-resolved photoluminescence spectra were recorded in THF to investigate the photoluminescence decay behaviors of these tetracoordinate boron-doped PAHs. As shown in Table 1 and Fig. 5, compounds **NBNN-1**, **NBNN-2** and **NBNN-3** consisted of prompt fluorescence with τ_{pf} = 1.26 ns, 1.89 ns and 1.60 ns and delayed emission with τ_{df} = 38.06 μs, 8.15 μs and 24.8 μs, respectively. The fully fused compounds **NBNN-1f** and **NBNN-2f**, the carbazole-based compound with a hydroxy group on boron **NBNN-4**, and indole-based compound **NBNN-5** only exhibited the prompt fluorescence component (τ_{pf} = 1.07 ns, 1.20 ns, 4.69 ns, 1.79 ns, respectively), likely due to the relatively large singlet-triplet band gap.

To further investigate the delayed fluorescence behaviors of **NBNN-1**–**NBNN-3**, Φ_{pl} and the lifetimes of the prompt/delayed components (τ_{pf}/τ_{df}) were exploited to estimate the photophysical rate constant of radiative decay (k_r), intersystem crossing (k_{ISC}), and reverse intersystem crossing of (k_{RISC}).[81] As shown in Table 2, the k_r value of **NBNN-2** (8.62×10^7 s^{-1}) is larger than those of **NBNN-1** (2.38×10^7 s^{-1}) and **NBNN-3** (3.94×10^7 s^{-1}). k_{ISC} (7.70×10^8 s^{-1}) and k_{RISC} (5.35×10^5 s^{-1}) of tetracoordinate boron-doped PAH **NBNN-1** with a phenyl group on the boron atom are the largest among those of **NBNN-1** to **NBNN-3**. The k_r value of **NBNN-2** (8.62×10^7 s^{-1}) is larger than those of **NBNN-1** (2.38×10^7 s^{-1}) and **NBNN-3** (3.94×10^7 s^{-1}). It is not clear why the different functional groups on the boron atom of the same skeleton could dramatically change k_{RISC}.

Molecules **NBNN-1** to **NBNN-5** displayed pseudo-reversible reduction peaks at ~−2.0 V (*vs.* Fc/Fc^+) and multiple reversible oxidation peaks with the first oxidation peaks at ~0.3 V (*vs.* Fc/Fc^+) (Table 1 and ESI†). The fused forms of boron-doped PAHs **NBNN-1f** and **NBNN-2f** show almost identical cyclic voltammograms as shown in Fig. 3c. The first oxidation peaks of **NBNN-1f** and **NBNN-2f** are lower than those of **NBNN-1** and **NBNN-2**, which can be attributed to the high-lying HOMO level (Fig. 4 bottom). The experimental data are in good agreement

Table 1 Photophysical and electrochemical data of **NBNN-1** to **NBNN-5**, **NBNN-1f** and **NBNN-2f**

	UV/vis[a]	Fluorescence			Phosphorescence[b]		Electrochemical data[c]	
	λ_{abs} (nm)	$\lambda_{em}{}^{a}$ (nm)/$\lambda_{em}{}^{b}$ (nm)	$\Phi_{pl}{}^{a,d}$ (%)/$\Phi_{pl}{}^{b,d}$ (%)	$\tau_{pf}{}^{a}$ (ns)/$\tau_{df}{}^{a}$ (μs)	λ_{em} (nm)	τ_{ph} (ms)	E_{red} (V)	E_{ox} (V)
NBNN-1	310, 469	557/556	62.3/55.7	1.26/38.06	569	302	−2.02	0.30
NBNN-1f	341, 376, 417, 457, 531	660/621	0.8/4.0	1.07/—[e]	643	0.012	−1.93	0.13
NBNN-2	308, 465	558/562	23.4/22.6	1.89/8.15	567	270	−2.16	0.26
NBNN-2f	332, 359, 404, 439, 528	659/624, 659	0.8/4.0	1.20/—[e]	638	5.62	−1.96	0.19
NBNN-3	309, 445, 481	564/561	24.5/26.6	1.60/24.8	583	213	−2.09	0.27
NBNN-4	304, 416, 461	551/556	34.8/25.3	4.69/—[e]	582	377	−2.06	0.28
NBNN-5	298, 370, 446	523/540	8.3/9.5	1.79/—[e]	569, 621	355	—[e]	—[e]

[a] 10^{-5} M in THF at 298 K. [b] PMMA film (10 wt%). [c] *vs.* Fc/Fc^{+} (ferrocene/ferrocenium) glassy carbon as the working electrode, a Pt wire as reference and counter electrodes, ferrocene (Fc/Fc^{+} = ferrocene/ferrocenium) was added to the solution as the internal reference, scan rate = 100 mV s^{-1}. [d] Quantum yields were determined using a calibrated integrating sphere. [e] Not available.

with the calculated HOMO and LUMO. Our previous study on tricoordinate boron-PAHs did not show such rich electrochemical properties.[80] After we measured the CV curves of the ligand **1a** and **1b** (Fig. 3c, S2.8 and S2.9†), we found that the ligand **1a** had similar multiple reversible oxidation peaks to the tetracoordinate boron-doped PAHs **NBNN-1**, **NBNN-1f** and **NBNN-2f**, as shown in Fig. 3c, which indicates that the ligand is likely ascribed to the multiple oxidation of **NBNN-1**, **NBNN-1f** and **NBNN-2f** rather than the introduction of the tetracoordinate boron atom. Compared to the reduction of ligands, the tetracoordinate boron-doped PAHs **NBNN-1**, **NBNN-1f** and **NBNN-2f** showed irreversible reduction at ~−2.00 V (*vs.* Fc/Fc^{+}), which indicates that the reduction peaks might originate from the boron atom.

Unlike the tricoordinate boron-doped PAH analogues in which the boron atom has a significant contribution to the LUMO and the HOMO/LUMO spread over the entire molecule,[80] the four-coordinate boron atom in **NBNN-1** to **NBNN-5**, **NBNN-**

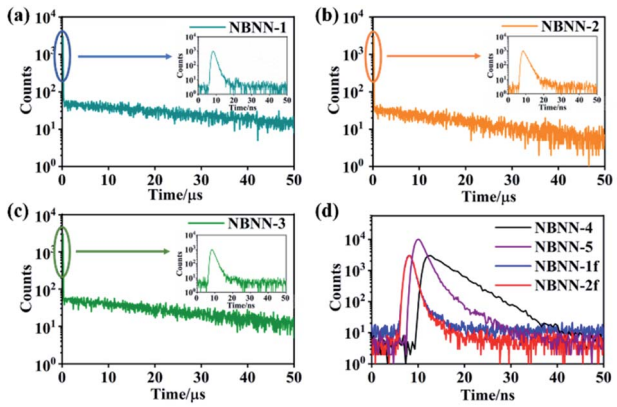

Fig. 5 (a)–(c) PL decay curves in THF under N_2 conditions at 298 K for **NBNN-1** to **NBNN-3**. (d) Transient fluorescence in THF under N_2 conditions at 298 K for **NBNN-4**, **NBNN-5**, **NBNN-1f** and **NBNN-2f**.

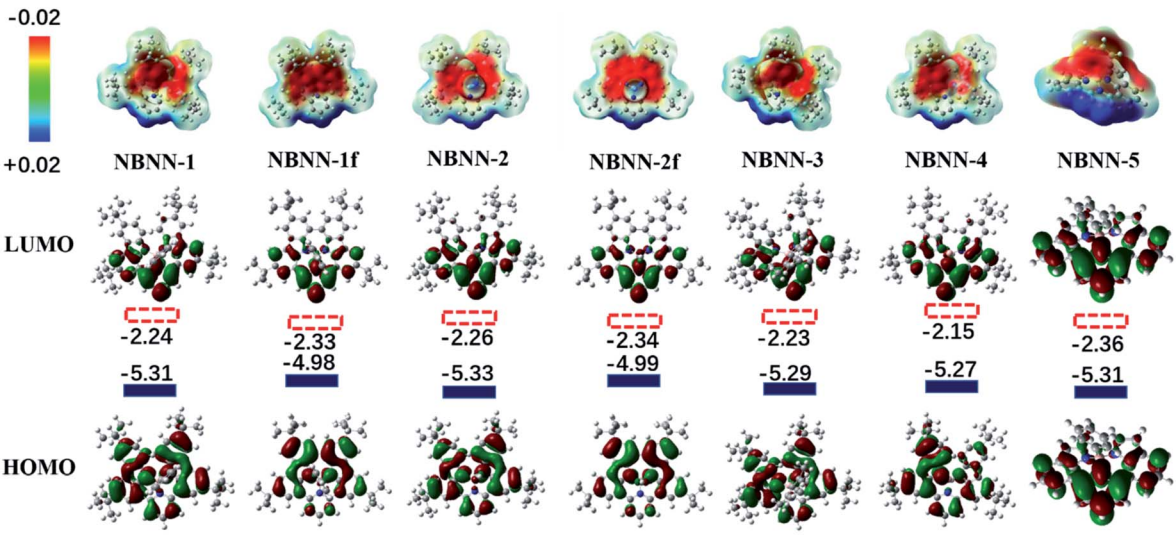

Fig. 4 Top: electrostatic potentials of tetracoordinate boron-doped PAHs **NBNN-1**–**NBNN-5**, **NBNN-1f**, and **NBNN-2f**. Bottom: DFT calculated energies and diagrams of the HOMO and LUMO for **NBNN-1**–**NBNN-5**, **NBNN-1f**, and **NBNN-2f** at the B3LYP/6-311g(d,p) level.

Table 2 The delayed fluorescence properties of NBNN-1 to NBNN-3 in THF solution[a]

Cmpd	τ_{pf}[b] (ns)/τ_{df}[b] (μs)	Φ_{pf}/Φ_{df}[c] (%)	k_r[d] (10^7 s^{-1})	k_{ISC}[e] (10^8 s^{-1})	k_{RISC}[f] (10^5 s^{-1})
NBNN-1	1.26/38.06	3.0/59.3	2.38	7.70	5.35
NBNN-2	1.89/8.15	16.3/7.1	8.62	4.43	0.64
NBNN-3	1.60/24.8	6.3/18.2	3.94	5.86	1.24

[a] Measured to be 10^{-5} M in THF for **NBNN-1** to **NBNN-2** at 298 K. [b] Emission lifetime for prompt (τ_{pf}) and delayed (τ_{df}) fluorescence. [c] Quantum yields for prompt (Φ_{pf}) and delayed (Φ_{df}) fluorescence, $\Phi_{pf} + \Phi_{df} = \Phi_{pl}$. [d] Rate constant of fluorescence radiative decay ($S_1 \rightarrow S_0$): $k_r = \Phi_{pf}/\tau_{pf}$. [e] Rate constant of ISC ($S_1 \rightarrow T_1$): $k_{ISC} = (1 - \Phi_{pf})/\tau_{pf}$. [f] Rate constant of RISC (T_1/S_1): $k_{RISC} = \Phi_{df}/k_{ISC}\tau_{pf}\tau_{df}\Phi_{pf}$.

1f and **NBNN-2f** has no contribution to the LUMO (Fig. 4), and their LUMO is mainly located on the pyridine and phenyl rings of carbazole and indole connected to pyridine. The calculated HOMO and LUMO prove that the substituents on the four-coordinate boron atom have trivial adjustment on the frontier molecular orbitals. Compared to **NBNN-1** and **NBNN-2**, **NBNN-1f** and **NBNN-2f** have smaller HOMO–LUMO gaps due to the notably elevated HOMO and slightly lowered LUMO, which could indicate the reason why the fused product **NBNN-4f** of **NBNN-4** was less stable and slowly decomposed on silica gel or alumina (Scheme 3). We note that the electrostatic potential maps of **NBNN-1–NBNN-5**, **NBNN-1f** and **NBNN-2f** display the development of negative characteristics on the tetracoordinate boron area and positive characteristics on the pyridine unit (Fig. 4 top).

To illustrate the aromaticity of these tetracoordinate boron-doped PAHs, the nucleus-independent chemical shift (NICS(1))[82,83] of two C3NBN rings and the 7-memebered C4NBN ring (if exists) around boron atoms was calculated (Fig. 6a, b and ESI†). The two C3NBN rings in **NBNN-1–NBNN-5** have positive NICS(1) values (see the ESI†), supporting their anti-aromaticity. The two C3NBN rings in **NBNN-1f** and **NBNN-2f** have much more positive NICS(1) values than those of **NBNN-1–NBNN-5**, indicating that they are more antiaromatic. Similar to the tricoordinate boron-doped PAH,[80] the 7-membered C4NBN has a larger NICS(1) value of 13.8 ppm (Fig. 6b). The anisotropy of the induced current density (ACID) calculations[84,85] (Fig. 6a and b) that are based on the optimized structures further showed that there is no electron density around the boron atom and the central 13-membered C4NC3NC3N ring of **NBNN-1f** is antiaromatic with an anti-clockwise diatropic ring current circuit.

The fused molecules **NBNN-1f** and **NBNN-2f** exhibited AIE behavior,[86,87] while compounds **NBNN-1–NBNN-5** only have normal photoluminescence properties. AIE behaviors of **NBNN-1f** and **NBNN-2f** are probably due to their structure constraint. We used **NBNN-1f** as an example to investigate the AIE phenomenon in detail (Fig. 6c–f). The red emission became stronger after the water content reached 50% in volume in THF, and the emission intensity grew faster when water was further added, as shown in Fig. 6c and e. The THF solution with 90% water displayed bright red emission. The quantum yields gradually increased when the water fraction increased. In addition, we found that the AIE behavior of **NBNN-1f** was accompanied by the blue-shift of emission (Fig. 6c). The photoluminescence decays only slightly increased when the water

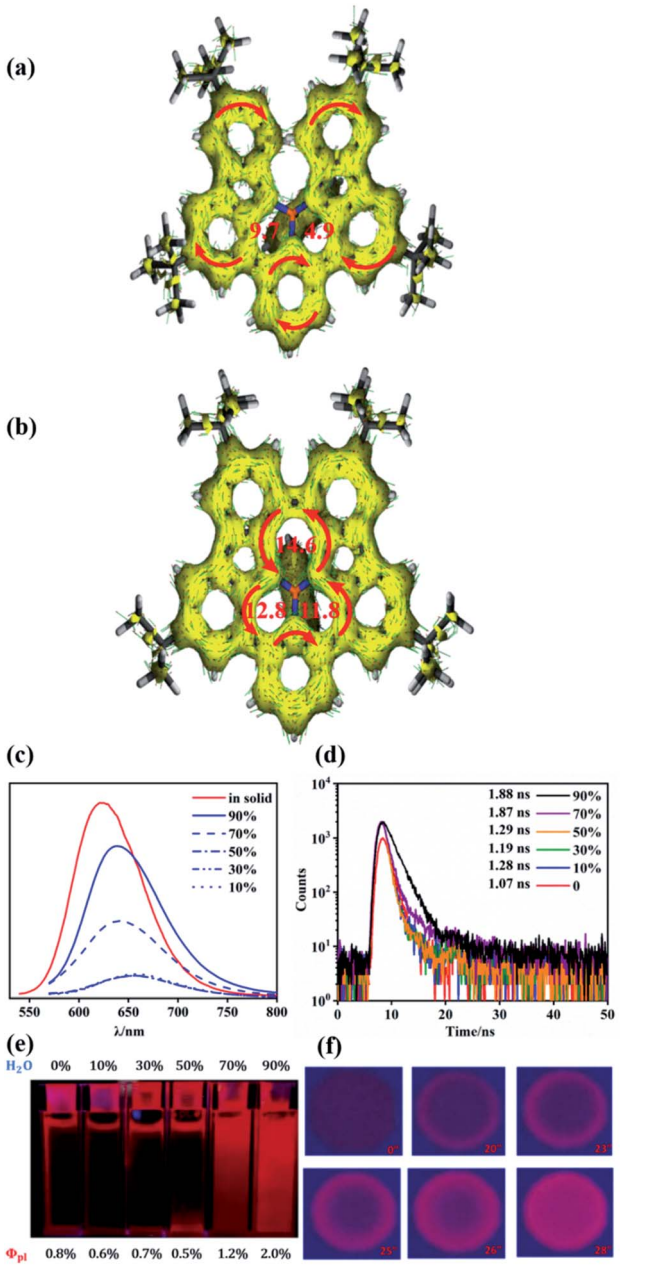

Fig. 6 (a) and (b) ACID plots of **NBNN-1** and **NBNN-1f**, and numbers in red representing NICS(1) in ppm. (c) Emission spectrum change of **NBNN-1f** in THF with different H_2O fractions (vol%). (d) Transient fluorescence curves in THF with different H_2O fractions (vol%). (e) Photographs showing the emission intensity increase with increasing H_2O fraction. (f) Photographs showing one drop of **NBNN-1f** solution on a thin-layer chromatography plate with different evaporation timescales.

fractions reached 70% and 90%, as shown in Fig. 6d. The AIE behavior of **NBNN-1f** was further demonstrated through change of emission intensity after adding one drop of **NBNN-1f** THF solution on a thin-layer chromatography plate (Fig. 6f). We observed a notable increase of the red emission under 365 nm UV lamp irradiation.

Conclusions

We developed an efficient strategy to construct a series of tetracoordinate boron-doped PAHs with various substituents on boron atoms at room temperature. Some of them were successfully converted to fully fused four-coordinate boron-doped NBN-PAHs *via* oxidative coupling. The tetracoordinate boron-doped PAHs exhibited delayed fluorescence. All the rings with tetracoordinate boron atoms are antiaromatic. The fused NBN-PAHs displayed blue-shifted AIE behavior.

Data availability

The data sets supporting this article have been uploaded as part of the ESI.†

Author contributions

L. J., B. Z. and D.-T. Yang conceptualized the work. L. J. developed the methodology and designed experiments. Y. W. recorded the time-resolved emission spectra. D. T. synthesized **NBNN-3**. X. C. and T. M. performed DFT calculations. D.-T. Y. wrote the original draft and created the original visuals. L. J., B. Z. and D.T. Y. edited the draft and visuals.

Conflicts of interest

There are no conflicts to declare.

Acknowledgements

The authors thank the National Natural Science Foundation of China (22001211) and Northwestern Polytechnical University for financial support. This project is also supported by special fund of Shaanxi Key Laboratory of Special Fuel Chemistry and Material (SPCF-SKL-2021-0014) and the Fundamental Research Funds for the Central Universities. The authors thank Prof. Lijie Liu, Dr Xiang Wang and Dr Guoyun Meng for insightful discussion.

Notes and references

1 X. Feng, J. Wu, M. Ai, W. Pisula, L. Zhi, J. P. Rabe and K. Müllen, *Angew. Chem., Int. Ed.*, 2007, **46**, 3033–3036.
2 M. Takase, V. Enkelmann, D. Sebastiani, M. Baumgarten and K. Müllen, *Angew. Chem., Int. Ed.*, 2007, **46**, 5524–5527.
3 J. Wei, B. Han, Q. Guo, X. Shi, W. Wang and N. Wei, *Angew. Chem., Int. Ed.*, 2010, **49**, 8209–8213.
4 T. Hatakeyama, S. Hashimoto, S. Seki and M. Nakamura, *J. Am. Chem. Soc.*, 2011, **133**, 18614–18617.
5 Z. Zhou, A. Wakamiya, T. Kushida and S. Yamaguchi, *J. Am. Chem. Soc.*, 2012, **134**, 4529–4532.
6 X. Wang, F. Zhang, J. Liu, R. Tang, Y. Fu, D. Wu, Q. Xu, X. Zhuang, G. He and X. Feng, *Org. Lett.*, 2013, **15**, 5714–5717.
7 L. Zou, X.-Y. Wang, K. Shi, J.-Y. Wang and J. Pei, *Org. Lett.*, 2013, **15**, 4378–4381.
8 E. Gońka, P. J. Chmielewski, T. Lis and M. Stępień, *J. Am. Chem. Soc.*, 2014, **136**, 16399–16410.
9 V. M. Hertz, M. Bolte, H.-W. Lerner and M. Wagner, *Angew. Chem., Int. Ed.*, 2015, **54**, 8800–8804.
10 H. Oshima, A. Fukazawa, T. Sasamori and S. Yamaguchi, *Angew. Chem., Int. Ed.*, 2015, **54**, 7636–7639.
11 M. Hirai, N. Tanaka, M. Sakai and S. Yamaguchi, *Chem. Rev.*, 2019, **119**, 8291–8331.
12 N. Ando, T. Yamada, H. Narita, N. N. Oehlmann, M. Wagner and S. Yamaguchi, *J. Am. Chem. Soc.*, 2021, **143**, 9944–9951.
13 Z. Liu and T. B. Marder, *Angew. Chem., Int. Ed.*, 2008, **47**, 242–244.
14 J. F. Araneda, B. Neue and W. E. Piers, *Angew. Chem., Int. Ed.*, 2012, **51**, 9977–9979.
15 J. S. A. Ishibashi, J. L. Marshall, A. Mazière, G. J. Lovinger, B. Li, L. N. Zakharov, A. Dargelos, A. Graciaa, A. Chrostowska and S.-Y. Liu, *J. Am. Chem. Soc.*, 2014, **136**, 15414–15421.
16 M. Krieg, F. Reicherter, P. Haiss, M. Ströbele, K. Eichele, M.-J. Treanor, R. Schaub and H. F. Bettinger, *Angew. Chem., Int. Ed.*, 2015, **54**, 8284–8286.
17 J. Dosso, J. Tasseroul, F. Fasano, D. Marinelli, N. Biot, A. Fermi and D. Bonifazi, *Angew. Chem., Int. Ed.*, 2017, **56**, 4483–4487.
18 K. Matsui, S. Oda, K. Yoshiura, K. Nakajima, N. Yasuda and T. Hatakeyama, *J. Am. Chem. Soc.*, 2018, **140**, 1195–1198.
19 S. Nakatsuka, N. Yasuda and T. Hatakeyama, *J. Am. Chem. Soc.*, 2018, **140**, 13562–13565.
20 S. Limberti, L. Emmett, A. Trandafir, G. Kociok-Köhn and G. D. Pantoş, *Chem. Sci.*, 2019, **10**, 9565–9570.
21 J. Hoffmann, B. Geffroy, E. Jaques, M. Hissler and A. Staubitz, *J. Mater. Chem. C*, 2021, **9**, 14720–14729.
22 A. Stock and E. Pohland, *Chem. Ges.*, 1926, **59**, 2215–2223.
23 M. Fingerle, C. Maichle-Mössmer, S. Schundelmeier, B. Speiser and H. F. Bettinger, *Org. Lett.*, 2017, **19**, 4428–4431.
24 D. Shimizu, K. Furukawa and A. Osuka, *Angew. Chem., Int. Ed.*, 2017, **56**, 7435–7439.
25 J. Huang and Y. Li, *Front. Chem.*, 2018, **6**, 341.
26 J.-K. Li, X.-Y. Chen, Y.-L. Guo, X.-C. Wang, A. C. H. Sue, X.-Y. Cao and X.-Y. Wang, *J. Am. Chem. Soc.*, 2021, **143**, 17958–17963.
27 J. Wang, X. Fang, X. Guo, Q. Wu, Q. Gong, C. Yu, E. Hao and L. Jiao, *Org. Lett.*, 2021, **23**, 4796–4801.
28 X.-Y. Wang, F.-D. Zhuang, X. Zhou, D.-C. Yang, J.-Y. Wang and J. Pei, *J. Mater. Chem. C*, 2014, **2**, 8152–8161.
29 S. K. Mellerup and S. Wang, *Trends Chem.*, 2019, **1**, 77–89.
30 R. Zhao, Y. Min, C. Dou, B. Lin, W. Ma, J. Liu and L. Wang, *ACS Appl. Polym. Mater.*, 2020, **2**, 19–25.
31 T. Hatakeyama, K. Shiren, K. Nakajima, S. Nomura, S. Nakatsuka, K. Kinoshita, J. Ni, Y. Ono and T. Ikuta, *Adv. Mater.*, 2016, **28**, 2777–2781.

32 H. Nakanotani, T. Furukawa, T. Hosokai, T. Hatakeyama and C. Adachi, *Adv. Opt. Mater.*, 2017, **5**, 1700051.
33 H. Fukagawa, T. Oono, Y. Iwasaki, T. Hatakeyama and T. Shimizu, *Mater. Chem. Front.*, 2018, **2**, 704–709.
34 X. Liang, Z.-P. Yan, H.-B. Han, Z.-G. Wu, Y.-X. Zheng, H. Meng, J.-L. Zuo and W. Huang, *Angew. Chem., Int. Ed.*, 2018, **57**, 11316–11320.
35 G. Meng, X. Chen, X. Wang, N. Wang, T. Peng and S. Wang, *Adv. Opt. Mater.*, 2019, **7**, 1970043.
36 J. U. Kim, I. S. Park, C.-Y. Chan, M. Tanaka, Y. Tsuchiya, H. Nakanotani and C. Adachi, *Nat. Commun.*, 2020, **11**, 1765.
37 Y. H. Lee, Y.-S. Shin, T. Lee, J. Jung, J.-H. Lee and M. H. Lee, *Chem. Eng. J.*, 2021, **423**, 130224.
38 M. Stępień, E. Gońka, M. Żyła and N. Sprutta, *Chem. Rev.*, 2017, **117**, 3479–3716.
39 A. Borissov, Y. K. Maurya, L. Moshniaha, W.-S. Wong, M. Żyła-Karwowska and M. Stępień, *Chem. Rev.*, 2022, **122**, 565–788.
40 X.-Y. Wang, F.-D. Zhuang, X.-C. Wang, X.-Y. Cao, J.-Y. Wang and J. Pei, *Chem. Commun.*, 2015, **51**, 4368–4371.
41 M. Numano, N. Nagami, S. Nakatsuka, T. Katayama, K. Nakajima, S. Tatsumi, N. Yasuda and T. Hatakeyama, *Chem.–Eur. J.*, 2016, **22**, 11574–11577.
42 S. K. Mellerup, C. Li, T. Peng and S. Wang, *Angew. Chem., Int. Ed.*, 2017, **56**, 6093–6097.
43 Y. Fu, X. Chang, H. Yang, E. Dmitrieva, Y. Gao, J. Ma, L. Huang, J. Liu, H. Lu, Z. Cheng, S. Du, H.-J. Gao and X. Feng, *Angew. Chem., Int. Ed.*, 2021, **60**, 26115–26121.
44 M. Zhao and Q. Miao, *Angew. Chem., Int. Ed.*, 2021, **60**, 21289–21294.
45 T. Agou, J. Kobayashi and T. Kawashima, *Org. Lett.*, 2006, **8**, 2241–2244.
46 F. Qiu, F. Zhang, R. Tang, Y. Fu, X. Wang, S. Han, X. Zhuang and X. Feng, *Org. Lett.*, 2016, **18**, 1398–1401.
47 Z.-C. He, S. K. Mellerup, L. Liu, X. Wang, C. Dao and S. Wang, *Angew. Chem., Int. Ed.*, 2019, **58**, 6683–6687.
48 Y. Chen, W. Chen, Y. Qiao, X. Lu and G. Zhou, *Angew. Chem., Int. Ed.*, 2020, **59**, 7122–7130.
49 S. M. Suresh, E. Duda, D. Hall, Z. Yao, S. Bagnich, A. M. Z. Slawin, H. Bässler, D. Beljonne, M. Buck, Y. Olivier, A. Köhler and E. Zysman-Colman, *J. Am. Chem. Soc.*, 2020, **142**, 6588–6599.
50 D. Shimoyama, N. Baser-Kirazli, R. A. Lalancette and F. Jäkle, *Angew. Chem., Int. Ed.*, 2021, **60**, 17942–17946.
51 X. Wang, F. Zhang, J. Gao, Y. Fu, W. Zhao, R. Tang, W. Zhang, X. Zhuang and X. Feng, *J. Org. Chem.*, 2015, **80**, 10127–10133.
52 X.-Y. Wang, A. Narita, X. Feng and K. Müllen, *J. Am. Chem. Soc.*, 2015, **137**, 7668–7671.
53 Q. Zhang, Z. Sun, L. Zhang, M. Li, L. Zi, Z. Liu, B. Zhen, W. Sun and X. Liu, *J. Org. Chem.*, 2020, **85**, 7877–7883.
54 P.-F. Zhang, J.-C. Zeng, F.-D. Zhuang, K.-X. Zhao, Z.-H. Sun, Z.-F. Yao, Y. Lu, X.-Y. Wang, J.-Y. Wang and J. Pei, *Angew. Chem., Int. Ed.*, 2021, **60**, 23313–23319.
55 T. Hatakeyama, S. Hashimoto, T. Oba and M. Nakamura, *J. Am. Chem. Soc.*, 2012, **134**, 19600–19603.
56 N. Ando, H. Soutome and S. Yamaguchi, *Chem. Sci.*, 2019, **10**, 7816–7821.
57 J. Wang, N. Wang, G. Wu, S. Wang and X. Li, *Angew. Chem., Int. Ed.*, 2019, **58**, 3082–3086.
58 N. Baser-Kirazli, R. A. Lalancette and F. Jäkle, *Angew. Chem., Int. Ed.*, 2020, **59**, 8689–8697.
59 J. Guo, Y. Yang, C. Dou and Y. Wang, *J. Am. Chem. Soc.*, 2021, **143**, 18272–18279.
60 F. D. Zhuang, J. H. Yang, Z. H. Sun, P. F. Zhang, Q. R. Chen, J. Y. Wang and J. Pei, *Chin. J. Chem.*, 2021, **39**, 909–912.
61 J. F. Araneda, W. E. Piers, B. Heyne, M. Parvez and R. McDonald, *Angew. Chem., Int. Ed. Engl.*, 2011, **50**, 12214–12217.
62 C. G. Claessens, D. González-Rodríguez, M. S. Rodríguez-Morgade, A. Medina and T. Torres, *Chem. Rev.*, 2014, **114**, 2192–2277.
63 S. Shimizu, *Chem. Rev.*, 2017, **117**, 2730–2784.
64 Y. Min, C. Dou, H. Tian, Y. Geng, J. Liu and L. Wang, *Angew. Chem., Int. Ed.*, 2018, **57**, 2000–2004.
65 S. Mula, N. Leclerc, P. Leveque, P. Retailleau and G. Ulrich, *J. Org. Chem.*, 2018, **83**, 14406–14418.
66 D. Cappello, R. R. Maar, V. N. Staroverov and J. B. Gilroy, *Chem.–Eur. J.*, 2020, **26**, 5522–5529.
67 K. Matsuo, S. Saito and S. Yamaguchi, *J. Am. Chem. Soc.*, 2014, **136**, 12580–12583.
68 K. Matsuo, S. Saito and S. Yamaguchi, *Angew. Chem., Int. Ed.*, 2016, **55**, 11984–11988.
69 S. Osumi, S. Saito, C. Dou, K. Matsuo, K. Kume, H. Yoshikawa, K. Awaga and S. Yamaguchi, *Chem. Sci.*, 2016, **7**, 219–227.
70 S. Oda, T. Shimizu, T. Katayama, H. Yoshikawa and T. Hatakeyama, *Org. Lett.*, 2019, **21**, 1770–1773.
71 Y. Sato, Y. Goto, K. Nakamura, Y. Miyamoto, Y. Sumida and H. Ohmiya, *ACS Catal.*, 2021, **11**, 12886–12892.
72 H. Gotoh, S. Nakatsuka, H. Tanaka, N. Yasuda, Y. Haketa, H. Maeda and T. Hatakeyama, *Angew. Chem., Int. Ed.*, 2021, **60**, 12835–12840.
73 S. Nakatsuka, H. Gotoh, K. Kinoshita, N. Yasuda and T. Hatakeyama, *Angew. Chem., Int. Ed.*, 2017, **56**, 5087–5090.
74 S. A. Iqbal, J. Pahl, K. Yuan and M. J. Ingleson, *Chem. Soc. Rev.*, 2020, **49**, 4564–4591.
75 P. B. Pati, E. Jin, Y. Kim, Y. Kim, J. Mun, S. J. Kim, S. J. Kang, W. Choe, G. Lee, H.-J. Shin and Y. S. Park, *Angew. Chem., Int. Ed.*, 2020, **59**, 14891–14895.
76 S. Oda and T. Hatakeyama, *Bull. Chem. Soc. Jpn.*, 2021, **94**, 950–960.
77 J.-S. Lu, S.-B. Ko, N. R. Walters, Y. Kang, F. Sauriol and S. Wang, *Angew. Chem., Int. Ed.*, 2013, **52**, 4544–4548.
78 D.-T. Yang, S. K. Mellerup, X. Wang, J.-S. Lu and S. Wang, *Angew. Chem., Int. Ed.*, 2015, **54**, 5498–5501.
79 S. Wang, D.-T. Yang, J. Lu, H. Shimogawa, S. Gong, X. Wang, S. K. Mellerup, A. Wakamiya, Y.-L. Chang, C. Yang and Z.-H. Lu, *Angew. Chem., Int. Ed.*, 2015, **54**, 15074–15078.
80 D. T. Yang, T. Nakamura, Z. He, X. Wang, A. Wakamiya, T. Peng and S. Wang, *Org. Lett.*, 2018, **20**, 6741–6745.

81 G. Meng, L. Liu, Z. He, D. Hall, X. Wang, T. Peng, X. Yin, P. Chen, D. Beljonne, Y. Olivier, E. Zysman-Colman, N. Wang and S. Wang, *Chem. Sci.*, 2022, **13**, 1665–1674.
82 P. v. R. Schleyer, C. Maerker, A. Dransfeld, H. Jiao and N. J. R. van Eikema Hommes, *J. Am. Chem. Soc.*, 1996, **118**, 6317–6318.
83 P. v. R. Schleyer, M. Manoharan, Z.-X. Wang, B. Kiran, H. Jiao, R. Puchta and N. J. R. van Eikema Hommes, *Org. Lett.*, 2001, **3**, 2465–2468.
84 D. G. R. Herges, *J. Phys. Chem. A*, 2001, 3214–3220.
85 K. H. D. Geuenich, F. Kohler and R. Herges, *Chem. Rev.*, 2005, **105**, 3758–3772.
86 J. Luo, Z. Xie, J. W. Y. Lam, L. Cheng, H. Chen, C. Qiu, H. S. Kwok, X. Zhan, Y. Liu, D. Zhu and B. Z. Tang, *Chem. Commun.*, 2001, 1740–1741.
87 J. Mei, N. L. C. Leung, R. T. K. Kwok, J. W. Y. Lam and B. Z. Tang, *Chem. Rev.*, 2015, **115**, 11718–11940.